Design of Engineered Heart Tissues to Minimize Arrhythmic Risk After Implantation in Infarcted Hearts

Ricardo M Rosales[1,2], Manuel Doblaré[1,2], Manuel M Mazo[3,4], Esther Pueyo[1,2]

[1] Aragon Institute of Engineering Research, University of Zaragoza, IIS Aragon, Zaragoza, Spain
[2] CIBER in Bioengineering, Biomaterials & Nanomedicine (CIBER-BBN), Spain
[3] Regenerative Medicine Program, CIMA Universidad de Navarra, Pamplona, Spain
[4] Hematology and Cell Therapy, Clínica Universidad de Navarra, Pamplona, Spain

Abstract

Implantation of engineered heart tissues (EHTs) built from human induced pluripotent stem cell-derived cardiomyocytes (hiPSC-CMs) may restore cardiac function after myocardial infarction (MI). However, this might entail high arrhythmic risk due to poor electrical coupling and cellular organization in the EHTs.

We used an in silico porcine-specific biventricular (BiV) model of MI with an engrafted EHT and we assessed the impact of the EHT electrical conductivity (EHTc) (10%*,* 50% *and* 90% *of that in healthy myocardium) and the hiPSC-CM alignment (EHTal) (random, parallel and perpendicular to the nearby epicardium) on the electrophysiological properties of the coupled BiV-EHT model.*

Results showed that the action potential duration (APD) in the EHT was largely driven by the APD in the host tissue, especially for the highest EHTc. Besides, higher EHTc values led to lower repolarization time gradients (RTGs) in the coupled BiV-EHT model, thus implying lower arrhythmic risk. In mean for all tested EHTal cases, the maximum RTG was reduced by $72.4\,\mathrm{ms/mm}$ *when EHTc was increased from* 10% *to* 90%*. Varying EHTal had minor electrophysiological effects on the engrafted EHT.*

In conclusion, proarrhythmicity after EHT engraftment on infarcted ventricles highly depends on EHTc while EHTal plays a negligible role.

1. Introduction

The functional remodeling that occurs following myocardial infarction (MI) involves a reduction in the conduction velocity (CV), longer action potentials (APs) and a reduced left ventricular ejection fraction, among other electro-mechanical alterations [1]. Tissue engineering techniques involving the implantation of human induced pluripotent stem cell-derived cardiomyocytes (hiPSC-CMs) on the MI region have shown promising results in restoring the reduced contractility of the ventricular myocardium [2], but the immature phenotype of these cells has raised concerns regarding the risk for arrhythmias.

The immaturity of hiPSC-CMs has been shown to be minimized by culturing the cells in bioprinted scaffolds to generate engineered heart tissues (EHTs) [3]. Nevertheless, the cells in the EHTs still present features that are different from those of adult ventricular cells. The CX43 expression in the hiPSC-CMs of the EHTs is reduced and presents a more isotropic distribution along the cell membrane. The hiPSC-CM organization in the EHT lacks the characteristic anisotropy of the adult ventricular tissue. All this leads to EHTs having reduced cell-to-cell coupling and lower conduction velocity (CV) than the healthy ventricular myocardium [2], on top of the hiPSC-CMs of the EHTs presenting a longer AP duration (APD) due to the distinct ionic contributions. Such electrophysiological properties contribute to the high proarrhythmic risk reported for tissue engineering therapies [4].

Extensive electrophysiological characterizations can nowadays benefit from the breakthrough in computing power and memory capacity, which has empowered computational modeling and simulation of cardiac electrical activity in healthy and pathological conditions [5]. Numerical simulations conducted using highly detailed biophysical models have aided in shedding light on the electrophysiological variables with the largest impact on cardiac proarrhythmicity while avoiding expensive and time consuming experiments and clinical trials [6, 7].

Here, we *in silico* evaluate the remuscularization of the infarcted ventricles by characterizing the changes in the electrophysiology of the coupled biventricular-EHT when the electrical conductivity (EHTc) and the alignment of the hiPSC-CMs (EHTal) in the EHTs are varied. This computational quantification extends our previous results [8] and enables identifying highly effective EHT design variables to improve the suitability of the remuscularization therapy.

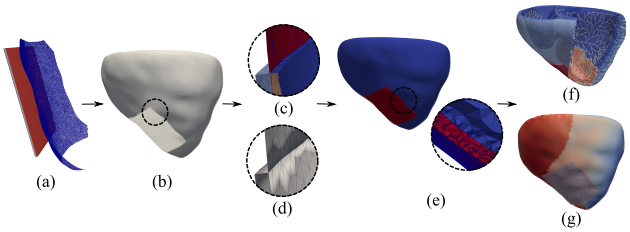

Figure 1: BiV-EHT model generation pipeline. (a) EHT and epicardial meshes (contact nodes in red). (b) Contacting BiV and EHT meshes. (c) Integrated BiV-EHT mesh with distinct regions and irregular triangles. (d) Cleaned BiV-EHT mesh. (e) Tetrahedral mesh with BiV (blue) and EHT (red) zones. BiV-EHT regions (f) and fiber field (g).

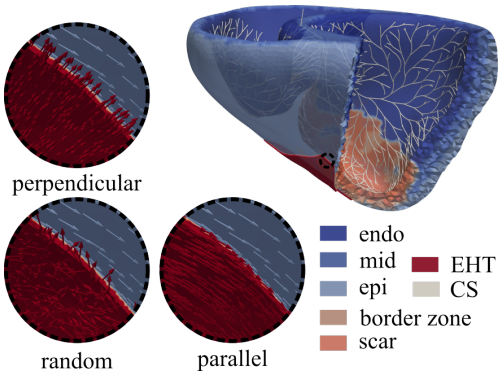

Figure 2: BiV-EHT model with the generated CS and transmural heterogeneities. The tested EHTal cases are shown on the left.

2. Materials and methods

2.1. Biventricular-EHT model generation

The detailed definition of our EHT-engrafted biventricular (BiV) model was presented previously [8]. In brief, we employed a late-gadolinium enhanced magnetic resonance image in combination with the full-width half-maximum method for the segmentation of the BiV model into healthy (HZ), border (BZ) and scar (SZ) zones. This MI-BiV domain was tetrahedralize with a mean edge length of $800\,\mu\mathrm{m}$ and its fiber field was obtained from a rule-based algorithm. The conduction system (CS) was defined by placing manual landmarks and interconnecting them using geodesic paths and a fractal tree algorithm. Moreover, the transmural heterogeneity was set by solving a multi-diffusion problem with a transmural proportion of 40:35:25 for the endo-, mid- and epicardium.

Next, we defined the BiV-EHT model as shown in Figure 1. Initially the EHT was defined as a superficial mesh of size $4\mathrm{x}4\mathrm{x}1\ \mathrm{mm}^3$ (Figure 1a). The sequential combination of a rigid and a non-rigid displacement were used for placing the EHT on top of the BiV epicardium, as depicted in Figure 1b. Then, we embedded half of the EHT into the BiV model and applied an *XOR* set operation for the integration of both superficial meshes (Figure 1c). As depicted in Figure 1d, irregular triangles on the interface were cleaned and the part of the EHT inner to the BiV mesh was erased. The BiV-EHT volume was meshed, with a tetrahedral mean edge length of 995 and 206 $\mu\mathrm{m}$ for the BiV and EHT regions, respectively. As shown in Figure 1f-g, the BiV tissue regions and fiber field were interpolated from the initial BiV model of MI.

2.2. Simulation setup

The biophysically detailed cellular models of O'Hara et al. [9], Paci et al. [10] and Stewart et al. [11] were employed for the definition of the HZ, the hiPSC-CM and CS APs, respectively. Besides, we modified the O'Hara et al. model to describe the decreased upstroke velocity and peak amplitude as well as the longer APD observed in the BZ [5]. Tissue electrical propagation was computed by numerically integrating the monodomain model with the in-house developed software *ELECTRA* [12]. Each organ level simulation consisted of three beats at $1\,\mathrm{Hz}$ pacing, with the last beat being used for the evaluation. Stimuli of $80\,\mathrm{mA}$-magnitude and $1\,\mathrm{ms}$-duration were applied at the CS atrioventricular node. The CS endpoints were connected to the ventricular nodes that were within $1\,\mathrm{mm}$ distance to define the Purkinje-muscular junctions.

All regions in the model were considered to have transverse isotropic conductivity. The HZ, BZ and CS longitudinal diffusion coefficients were set to 0.0013, 0.00095 and $0.01\ \mathrm{cm}^2/\mathrm{ms}$ (equivalent to 0.13, 0.095 and $1\ \mathrm{S}/\mathrm{m}$ for a membrane surface-to-volume ratio of $1000\ \mathrm{cm}^{-1}$ and capacitance per unit area of $1\ \mu\mathrm{F}/\mathrm{cm}^2$), respectively. The CS longitudinal diffusion coefficient was reduced near the CS endpoints to match the ventricular longitudinal conductivity. The SZ was defined as non-conductive. Transverse-to-longitudinal diffusion ratios were set to 0.25 for HZ and EHT and to 0.32 for BZ [5, 8].

We evaluated the EHT activation time (AT), APD at $90\,\%$ repolarization (APD_{90}), CV and repolarization time gradients (RTGs) from the numerically obtained transmembrane voltage [8].

2.3. EHT conductivity and cell alignment

To assess the electrophysiological impact of the maturation state and cell organization of the hiSPC-CMs cultured in bioprinted scaffolds, we concomitantly varied EHTc and EHTal in our *in silico* EHTs. For EHTc, we tested relative conductivities of 10%, 50% and 90% of that in healthy myocardium, which represent different levels of CX43 and

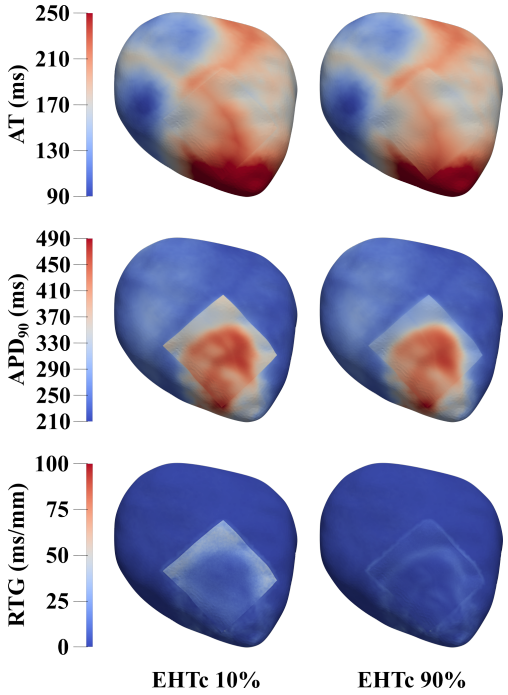

Figure 3: AT, APD_{90} and RTG maps for 10% and 90% relative EHTc and the random EHTal.

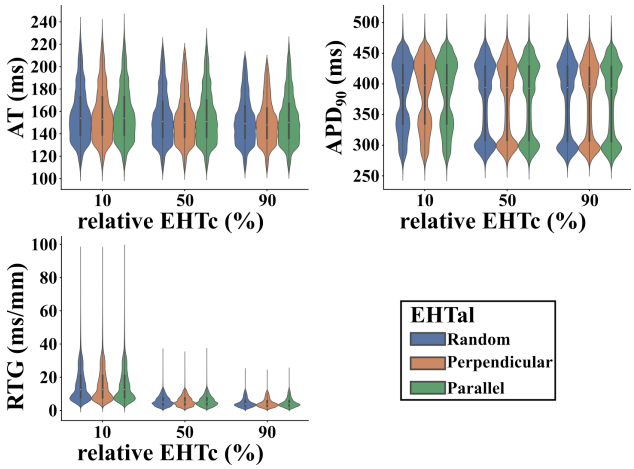

Figure 4: AT, APD_{90} and RTG distributions in the EHT for different EHTc and EHTal values.

their distributions on the cell membrane associated with different maturation degrees. For EHTal, we previously observed that minimal variations in the hiPSC-CM alignment had a negligible impact on the arrhythmic risk associated with the EHT implantation [13]. Therefore, we globally varied the hiPSC-CM orientation on the EHT by setting it to be random, parallel or perpendicular to the underneath epicardial cells, as depicted in Figure 2.

3. Results and discussion

We first investigated the impact of the EHT design variables on the depolarization properties of the EHT. We found that the ATs were almost unchanged for the different EHTal options, while they were slightly reduced when EHTc was increased. Qualitatively, the depolarization traveled from the lateral corners of the EHT towards its center and continued to the bottom corner for all tested EHTc and EHTal options (see Figure 3 for the random EHT alignment and EHTc values of 10% and 90%). Quantitatively, the mean CV over all EHTal options was 8.13, 24.17 and 31.1 $\mathrm{cm/s}$ for relative EHTc values of 10%, 50% and 90%, respectively. The largest variation in the maximum AT of the EHT was 31 ms when the EHTc was increased from 10% to 90% for the perpendicular EHTal, as shown in Figure 4. These results are in concordance with previous results by Yu et al. [6], Fassina et al. [7] and our group [8], which consistently showed that the host myocardium drives the depolarization of the completely engrafted EHT. Here, and in agreement with those results, we found a minimal EHTc-related variation in the ATs of the EHT (see Figure 3). As an example, only a minimal 11.2% decrement in the maximum AT (in mean over all EHTal options) was seen even after increasing the EHTc 9 times. This small variation in the maximum AT can be explained by the late activation of the EHT bottom corner, as the EHT bottom corner was hidden from the CS by the non-conductive SZ. Moreover, Fassina et al. [4] and our group [13] previously showed that the ATs in an EHT engrafted to a transmurally infarcted slab of ventricular tissue were highly influenced by the EHTc value. Taking all together, our results suggest that the driving of the EHT activation by the host myocardium is dependent on the combination of the host myocardium substrate and the EHT implantation location.

Regarding the impact of the EHT design on the repolarization, we found that the APD_{90} values in the EHT resembled the values found at the underneath host myocardium. This effect was more accentuated for higher EHTc values, as illustrated in Figure 3, since the highest 90% relative EHTc allowed a better EHT-myocardium electrical coupling than in the lowest 10% EHTc. In this scenario, the APD_{90} in the EHT regions in contact with the HZ and the BZ were reduced and maintained, respectively, due to the electrotonic load exerted by the host tissue to the EHT, as observed numerically [4, 13] and experimentally [14] in other studies. With regards to EHTal, we observed a null influence of the hiPSC-CMs alignment on the APD_{90}.

With respect to the arrhythmic risk marker RTG, its values were nearly constant for all EHTal cases. Other *in silico* studies have shown an RTG reduction when the hiPSC-CMs were aligned parallel to the myocardial propagation

in a transmurally infarcted tissue slab [13] and a variation in the arrhythmic burden for different hiPSC-CM alignment when the EHT was attached to two different locations of two BiV models with different MI substrates [6]. Thus, the effect of EHTal on arrhythmicity is highly dependent on the MI substrate and the EHT location. Importantly, we found EHTc to be a major contributor to RTG. The median RTG in the EHT was reduced with the increasing EHTc. In particular, the median RTGs on the EHT were 12.6, 5.1 and $3.9\ \mathrm{ms/mm}$ for the 10%, 50% and 90% EHTc, respectively, in mean over all EHTal cases. Also, the maximum RTG in the EHT decreased from 97.1 to $24.7\ \mathrm{ms/mm}$ for an increment of the EHTc from 10% to 90%, in mean over all EHTal cases. As in [8], the lowest value of the maximum RTG for the different EHTc cases ($24.7\ \mathrm{ms/mm}$) was markedly higher than the $3.2\ \mathrm{ms/mm}$ threshold shown to produce unidirectional blocks by Laurita et al. [15]. Based on these results, an increase in EHTc associated with higher hiPSC-CM maturation would be fundamental to minimize arrhythmogenecity after EHT engrafment.

4. Conclusion

The alignment of the hiPSC-CMs in an EHT has negligible effects while increased EHT electrical conductivity largely reduces proarrhythmic risk after engraftment in infarcted hearts.

Acknowledgments

This work was supported by EU H2020 Program under G.A. 874827 (BRAV3), by Ministerio de Ciencia e Innovación (Spain) through projects PID2019-105674RB-I00, PID2022-140556OB-I00, TED2021-130459B-I00 and CARDIOPRINT (PLEC2021-008127), by European Social Fund (EU) and Aragón Government through project LMP94_21 and BSICoS group T39_23R.

References

[1] Frantz S, Hundertmark MJ, Schulz-Menger J, Bengel FM, Bauersachs J. Left Ventricular Remodelling Post-Myocardial Infarction: Pathophysiology, Imaging, and Novel Therapies. European Heart Journal July 2022; 43:2549–2561.

[2] Zhao Y, Feric NT, Thavandiran N, Nunes SS, Radisic M. The Role of Tissue Engineering and Biomaterials in Cardiac Regenerative Medicine. Canadian Journal of Cardiology November 2014;30:1307–1322.

[3] Montero-Calle P, et al. Fabrication of Human Myocardium Using Multidimensional Modelling of Engineered Tissues. Biofabrication October 2022;14:045017.

[4] Fassina D, Costa CM, Longobardi S, Karabelas E, Plank G, Harding SE, Niederer SA. Modelling the Interaction Between Stem Cells Derived Cardiomyocytes Patches and Host Myocardium to Aid Non-Arrhythmic Engineered Heart Tissue Design. PLoS Comput Biol 2022; 18:e1010030.

[5] Lopez-Perez A, Sebastian R, Izquierdo M, Ruiz R, Bishop M, Ferrero JM. Personalized Cardiac Computational Models: From Clinical Data to Simulation of Infarct-Related Ventricular Tachycardia. Front Physiol 2019;10:580.

[6] Yu JK, et al. Assessment of Arrhythmia Mechanism and Burden of the Infarcted Ventricles Following Remuscularization With Pluripotent Stem Cell-Derived Cardiomyocyte Patches Using Patient-Derived Models. Cardiovascular Research 2022;118:1247–1261.

[7] Fassina D, M. Costa C, Bishop M, Plank G, Whitaker J, Harding SE, Niederer SA. Assessing the Arrhythmogenic Risk of Engineered Heart Tissue Patches Through In Silico Application on Infarcted Ventricle Models. Computers in Biology and Medicine 2023;154:106550.

[8] Rosales R, Mountris K, Doblaré M, Mazo M, Pueyo E. In Silico Assessment of Arrhythmic Risk in Infarcted Ventricles Engrafted with Engineered Heart Tissues. 2023 Computing in Cardiology November 2023;50:1–4.

[9] O'Hara T, Virág L, Varró A, Rudy Y. Simulation of the Undiseased Human Cardiac Ventricular Action Potential: Model Formulation and Experimental Validation. PLoS Comput Biol 2011;7:e1002061.

[10] Paci M, Hyttinen J, Aalto-Setälä K, Severi S. Computational Models of Ventricular- and Atrial-Like Human Induced Pluripotent Stem Cell Derived Cardiomyocytes. Annals of Biomedical Engineering 2013;41:2334–2348.

[11] Stewart P, Aslanidi OV, Noble D, Noble PJ, Boyett MR, Zhang H. Mathematical Models of the Electrical Action Potential of Purkinje Fibre Cells. Phil Trans R Soc A 2009; 367(1896):2225–2255.

[12] Mountris KA, Pueyo E. A Dual Adaptive Explicit Time Integration Algorithm for Efficiently Solving the Cardiac Monodomain Equation. Int J Numer Method Biomed Eng 2021;37:e3461.

[13] Rosales RM, et al. Experimentally-Guided In Silico Design of Engineered Heart Tissues to Improve Cardiac Electrical Function After Myocardial Infarction. Computers in Biology and Medicine March 2024;171:108044.

[14] Zaniboni M, Pollard AE, Yang L, Spitzer KW. Beat-To-Beat Repolarization Variability in Ventricular Myocytes and Its Suppression by Electrical Coupling. American Journal of Physiology Heart and Circulatory Physiology 2000; 278:H677–H687.

[15] Laurita KR, Rosenbaum DS. Interdependence of Modulated Dispersion and Tissue Structure in the Mechanism of Unidirectional Block. Circulation Research 2000;87:922–928.

Address for correspondence:

Ricardo M. Rosales

University of Zaragoza, Campus Río Ebro, I+D Building, D-5.01.1B, Mariano Esquillor, s/n street, 50018, Zaragoza, Spain

rrosales@unizar.es